Journal of Chemical Health Risks

www.jchr.org

JCHR (2025) 15(1), 551-560 | ISSN:2251-6727

Structure Directing Amine Mediated Hydrothermal Synthesis of Mn Doped ZnO Microrods for Hazardous Methylene Blue Dye Degradation

K. Sasikumar,[a] M. Theanmozhi[a] and Robin Jude Vimal Michael[a*]

[a]Kinetics and Catalysis Lab (KCL), Abdul Kalam Research Centre (AKRC),

P.G. and Research Department of Chemistry, Sacred Heart College (Autonomous),

Tirupattur - 635601, Affiliated to Thiruvalluvar University, Serkkadu, Tamilnadu, India.

(Received: 16 November 2024 Revised: 11 December 2024 Accepted: 10 January 2025)

KEYWORDS
ZnO, Ethylenediamine, Structure directing amine, Hydrothermal, Hexagonal Microrods, Methylene blue dye, Environmental impact

ABSTRACT:

The controlled synthesis of Mn-doped ZnO nanospheres using an amine-mediated hydrothermal method was systematically investigated. X-ray diffraction (XRD) analysis confirmed the hexagonal wurtzite structure and phase purity of the synthesized samples, with crystallite sizes reducing significantly from 58 nm to 18 nm upon Mn doping, as calculated using the Williamson-Hall (W-H) plot method. Secondary XRD peaks indicated the successful incorporation of Mn ions on the ZnO surface. Fourier transform infrared (FTIR) spectroscopy further confirmed the presence of ZnO vibrations along with Mn-O bonding. UV-Vis diffuse reflectance spectroscopy (UV-DRS) analysis revealed a reduction in bandgap from 3.07 eV (pure ZnO) to 2.62 eV (Mn-doped ZnO), enhancing visible-light absorption. High-resolution scanning electron microscopy (HRSEM) and high-resolution transmission electron microscopy (HRTEM) confirmed the transformation of nanospheres into a microrod morphology and provided insights into particle size distribution, showing an average size of 32 nm for pure ZnO and 16.6 nm for Mn (5%)-doped ZnO. BET surface area analysis revealed a significant increase to 90 m2/g, which enhances light-harvesting efficiency and provides more active sites for catalytic applications. The photocatalytic performance was evaluated through methylene blue dye degradation under visible light, achieving an impressive 90.8% degradation efficiency. This study highlights the potential of Mn-doped ZnO nanospheres as an efficient photocatalyst for environmental remediation.

INTRODUCTION

The use of semiconductor materials for photocatalytic degradation of organic pollutants, such as dyes and pesticides, has gained significant attention in recent years [1-3]. Among these materials, zinc oxide (ZnO) stands out as a promising photocatalyst for both hydrogen generation and the breakdown of organic contaminants. This is due to its high exciton binding energy (60 meV) at room temperature, excellent photosensitivity, affordability, strong chemical stability, and low toxicity [4-7]. However, ZnO does have limitations. Its wide bandgap (3.37 eV) means it can only absorb UV light, making it ineffective at utilizing the vast majority (95-97%) of the solar spectrum [8]. Additionally, the rapid recombination of photogenerated electron-hole (e^-/h^+) pairs prevents optimal surface reactions needed to generate reactive oxygen species (ROS) such as hydroxyl radicals (•OH), superoxide ions ($O_2^{\bullet-}$), and hydrogen peroxide (H_2O_2), which are crucial for breaking down pollutants [9, 10]. To enhance ZnO photocatalytic performance in visible light, researchers have explored various strategies, including semiconductor coupling and doping [11-13].

Doping, which involves intentionally introducing impurities into the ZnO lattice, is one of the most effective ways to modify its optical and chemical properties [14, 15]. In specific, manganese doping has shown great promise. It introduces new energy states within ZnO bandgap, improving its ability to absorb visible light and facilitating better electron transitions between the valence bands (VB) and conduction bands (CB) [16-18]. This, in turn, helps to separate photogenerated charge carriers more efficiently, reducing recombination and enhancing photocatalytic

Journal of Chemical Health Risks

www.jchr.org

JCHR (2025) 15(1), 551-560 | ISSN:2251-6727

activity under visible light conditions [19]. Studies have consistently shown that Mn-doped ZnO (ZnO-Mn) exhibits superior photocatalytic performance under both UV and visible light compared to pure ZnO [20]. Factors such as particle morphology, size, defect concentration, and doping level all play a crucial role in determining how effectively ZnO-Mn can degrade organic dyes like methyl orange and methylene blue. With continued research and optimization, Mn-doped ZnO could become an even more powerful tool for sustainable water treatment and environmental cleanup [21, 22].

The present work investigates the degradation of methylene blue dye under visible light condition using Mn doped ZnO nanomaterials shows enhanced degradation efficiency when compared to pure ZnO synthesized by hydrothermal method.

MATERIALS AND METHODS

Materials. The reagents involved in the synthesis procedure are all from AR-grade and it is utilized without purification further. Pure ZnO and ZnO-Mn (1, 3 and 5%) materials were synthesized using zinc acetate dihydrate (Zn $(CH_3COO)_2 \cdot 2H_2O$, ≥99%, Merck) and manganese acetate tetra hydrate (Mn $(CH_3COO)_2 \cdot 4H_2O$ ≥99%, SRL). Ethylenediamine used as structure directing agent (Merck). Sodium hydroxide (NaOH, Merck) is used as a precipitating agent. A solution of methylene blue (MB) dye in double distilled water (DD) is used as a model wastewater.

Synthesis of Pure and Mn-ZnO Photocatalyst.

To prepare ZnO nanospheres decorated microrods, a solution containing 0.5 M zinc acetate dihydrate and 3 M sodium hydroxide was prepared by dissolving the chemicals in 50 mL of double distilled (DD) water. To this, 10 mL of ethylene diamine was added and the mixture was stirred continuously for 30 minutes. The solution was then transferred into a Teflon-lined stainless steel autoclave with a capacity of 150 mL. The total volume was adjusted to 80% of the autoclave capacity by adding more DD water. The autoclave, containing the prepared mixture, was placed in a hot air oven at 160 °C and left for 12 h to facilitate the reaction. After the autoclave cooled, the resulting zinc oxide precipitate was carefully separated from the solution, washed multiple times with DD water followed by ethanol to remove any residual impurities, and then dried at 80 °C to evaporate any remaining solvents. The same procedure was followed using manganese acetate as dopant and zinc acetate to produce ZnO-Mn samples with different manganese doping concentrations (1%, 3%, and 5%). The synthesized ZnO-Mn samples named as ZnO-Mn1%, ZnO-Mn3% and ZnO-Mn5%.

Photocatalytic degradation experiment with Mn doped ZnO

The photocatalytic degradation of Methylene blue dye using Mn doped ZnO as photocatalyst under the illumination of 500 W visible light source (Crown) was performed using an in-house fabricated photoreactor. The photoreactor setup consists of a magnetic stirrer with water flow and a source of visible light which is enclosed in a closed tight chamber. In a typical process, 0.30 g/L of catalyst was suspended in model wastewater of methylene blue dye solution. The solution was homogeneously dispersed using an ultrasonicator and kept at dark for 1 h in order to obtain absorption-desorption equilibrium. The suspension was kept magnetically stirred and illuminated with visible light source. Then the liquid samples were collected after a regular interval of time (15 min). The degradation of the dye was observed by measuring the absorbance spectrum of the solution in an UV-visible Spectrophotometer [23].

Materials characterization.

The X-ray diffraction (XRD) pattern was recorded using a Bruker D2 Phaser Diffractometer with a Cu-Kα source (1.540 Å) over a range of 20°-80°. The Fourier-transform infrared (FTIR) spectrum was obtained using a PerkinElmer instrument with the KBr pellet method. The bandgap of the material was measured using a JASCO V-670 PC spectrophotometer equipped with a Diffuse Reflectance Spectroscopy (DRS) attachment. The morphology and chemical composition of the sample were analyzed using a High-Resolution Scanning Electron Microscope (HR-SEM), FEI QUANTA 200 FEG, with a Schottky emitter (-200 V to 30 kV) and equipped with EDAX technology. High-Resolution Transmission Electron Microscopy (HRTEM) images of lattice fringes and the Selected Area Electron Diffraction (SAED) pattern were captured using a JEOL/JEM 2100 operating at 200 kV. X-ray Photoelectron Spectroscopy (XPS) was performed using an ULVAC-PHI, Inc. Model: PHI5000 Versaprobe III to determine the chemical state of the sample. The specific surface area

Journal of Chemical Health Risks

www.jchr.org

JCHR (2025) 15(1), 551-560 | ISSN:2251-6727

and pore volume were assessed through N_2 adsorption-desorption analysis using a Quantachrome Autosorb instrument. The photocatalytic dye degradation of methylene blue dye was done under Crown 500W visible light source.

RESULTS AND DISCUSSION

Phase and structural identification by X-Ray Diffraction.

The phase purity and structure of ZnO materials were investigated using X-Ray diffraction studies. Fig. 1a reveals the XRD pattern of pure and Mn5% doped ZnO nanomaterials synthesized by hydrothermal method. The predominant hkl planes (100), (002) and (101) for hexagonal wurtzite ZnO is well matched with the JCPDS card No: 36-1451 and space group of C6v or P63mc. [24] The crystallite size calculated from W-H plot in fig. 1b reveals the formation of nanomaterials with average particle size between 58 to 18 nm. For pure ZnO the particle size found to be 58 nm and while manganese introduced on the ZnO surface the particle size gets reduced significantly. With the increase in dopant concentration, the crystallite size of the sample decreases. The decrease in crystallite size is due to the distortion in host ZnO caused by the addition of Mn ions thereby decreasing grain growth and nucleation of Mn doped ZnO nanoparticles [25, 26]. Furthermore, in fig. 1c there are some secondary peaks around 18.2˚ observed in Mn5%-ZnO sample and it has a common region for (101) plane of $ZnMn_2O_4$ (18.2˚, JCPDS file:77-0470) and (111) plane of $ZnMnO_3$ (18.3˚, JCPDS file:19-1461) where the oxidation states of manganese are +3 and +4 respectively. The observed planes of (200) and (103) respectively at 30.6˚ and 33.2˚ confirm the formation of $ZnMn_2O_4$. From the fig. 1d inset shows formation of $ZnMnO_3$ is confirmed by the planes (220) and (400) at 30.2˚ and 43.4˚ respectively. The Zn^{2+} ion radius (0.74 Å) is higher than that of the Mn^{3+} (0.64 Å) and Mn^{4+} (0.62 Å) respectively. [27] However there is no major shift in the XRD peak position was observed when manganese included. This indicates that the Mn ions loaded on the ZnO Surface rather than interstitial position.

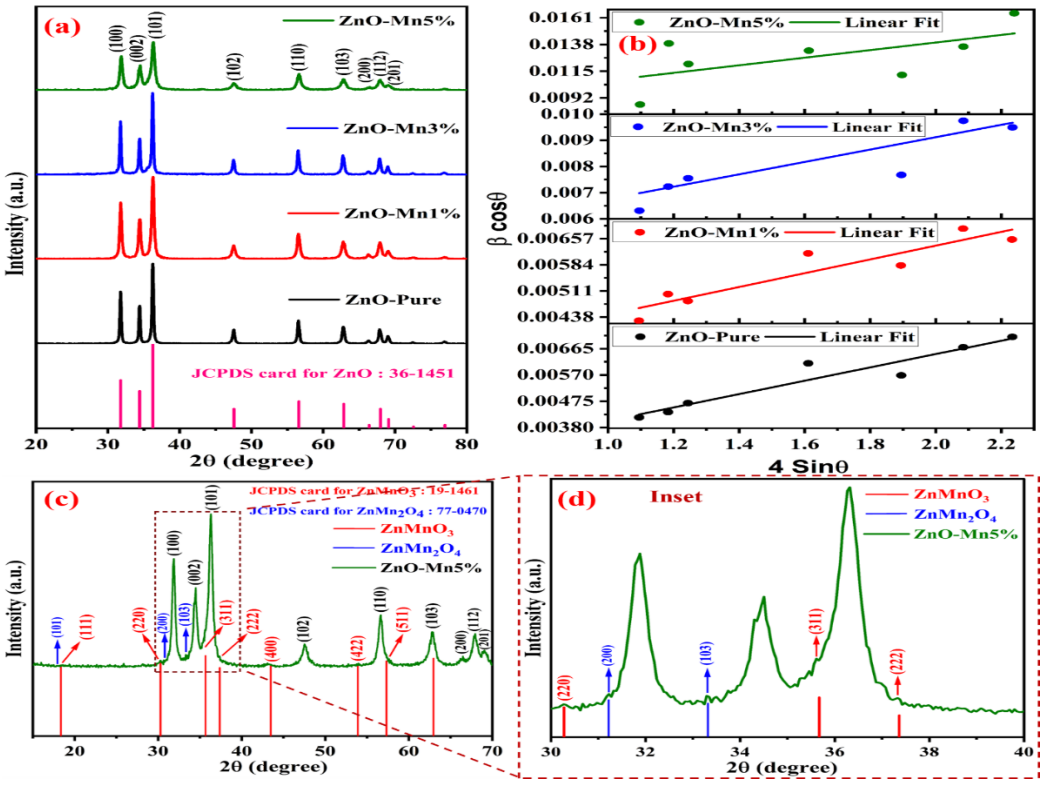

Figure 1. (a) XRD pattern of Pure and Mn-ZnO (1, 3 and 5%), (b) W-H plot, (c) ZnO-Mn5% showing Mn peaks (d) Inset for Mn peaks.

Journal of Chemical Health Risks

www.jchr.org

JCHR (2025) 15(1), 551-560 | ISSN:2251-6727

The lattice parameter values calculated for all ZnO materials reveals that a= 3.278 Å and c= 5.208 Å values are closer to the lattice constants of standard ZnO (a= 3.249 Å and c= 5.206 Å) which depicts that the synthesized pure and Mn-ZnO materials are in decent agreement with JCPDS cards. [28] The d-spacing value of 0.26 nm is assigned for (002) plane of ZnO.

Functional group identification by FTIR analysis.

To investigate the functional group and the molecular interactions in pure and Mn doped ZnO nanomaterials FTIR spectra were analyzed in the range of 400-4000 cm^{-1}.

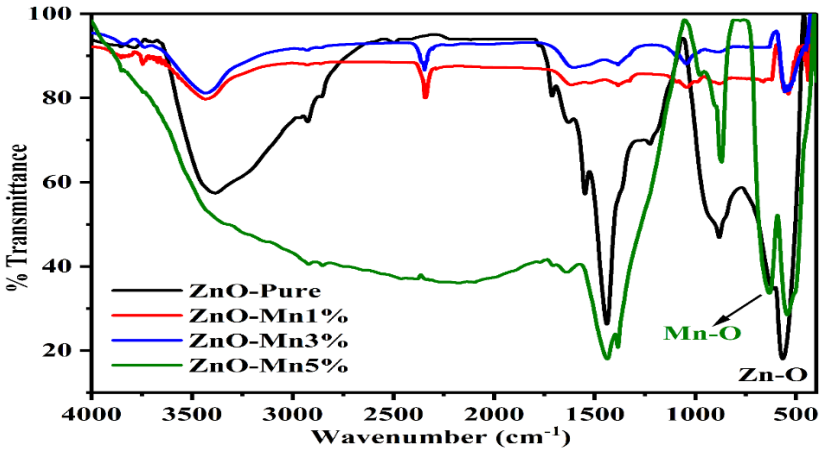

Figure 2. FTIR spectra of ZnO - Mn (0, 1, 3 and 5%).

Fig. 2 shows the peaks observed at 560 cm^{-1} in the pure ZnO nanomaterials confirms the formation of metal oxide bond which arise due to vibrational stretching of Zn-O bond [29]. A peak at 638 cm^{-1} is assigned to Mn-O of Mn doped ZnO samples. The absorption peak at 2335 cm^{-1} represents the C=O stretching mode. The peak at 2942 cm^{-1} corresponds to C-H bond [30, 31]. The hydroxyl group of metal oxide is present as broad peak in the range of 3387 cm^{-1} which arises due to stretching vibration of O-H bond [32].

Morphology and elemental compositional study by HRSEM-EDAX.

The morphology of the synthesized pure and Mn5% doped ZnO materials are revealed by HRSEM images shown in fig. 3a and b respectively. From fig. 3a the nanospheres developed as a microrod like morphology was observed and the elemental composition analysis of pure ZnO reveals the presence of Zn (80.6%) and O (19.4%).

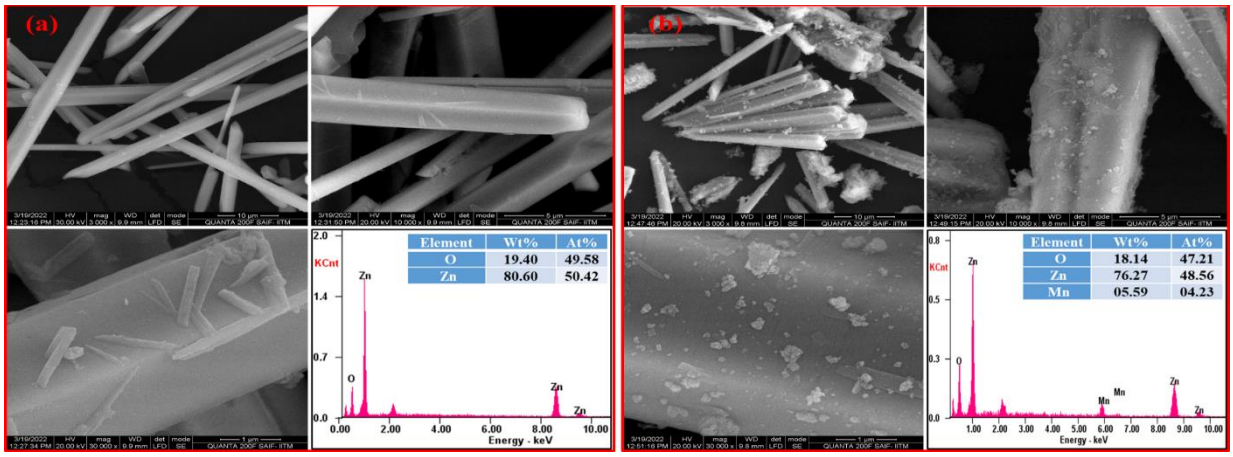

Figure 3. HRSEM images of (a) Pure ZnO and (b) Mn-ZnO microrods.

Journal of Chemical Health Risks

www.jchr.org

JCHR (2025) 15(1), 551-560 | ISSN:2251-6727

It is noteworthy, when manganese included in ZnO (Mn5%-ZnO) the morphology changes significantly with reduced particle size compared to pure ZnO. From fig. 3b it is clearly evidenced that the Mn ions deposited on the ZnO surface thereby reduced agglomeration and prevents the further microstructure growth. From the fig. 3b the EDAX spectrum displays the elemental concentration of Mn doped ZnO are calculated to be 76.2%, 18.1% and 5.6 for Zn, O and Mn respectively [33, 34].

ZnO and Mn Lattice observation using HRTEM analysis.

The High-Resolution Transmission Electron Microscopy (HRTEM) and Selected Area Electron Diffraction (SAED) are advanced tools used to examine the nanoscale structure, crystallinity, and lattice fringes of the materials. The HRTEM images of pure and Mn5% doped ZnO are shown in fig. 4a and b respectively. From the fig. 3a the nanosphere morphology of the materials was confirmed. The average particle size of the pure ZnO nanospheres calculated using Image J analytical tool and the particle size distribution histogram analysis reveals the appropriate size of 32 nm. The d-spacing between the lattice fringes calculate to be 0.26 nm for ZnO (002) plane. The SAED pattern displays a ring like pattern indicating the poly crystalline nature of the pure ZnO material [35].

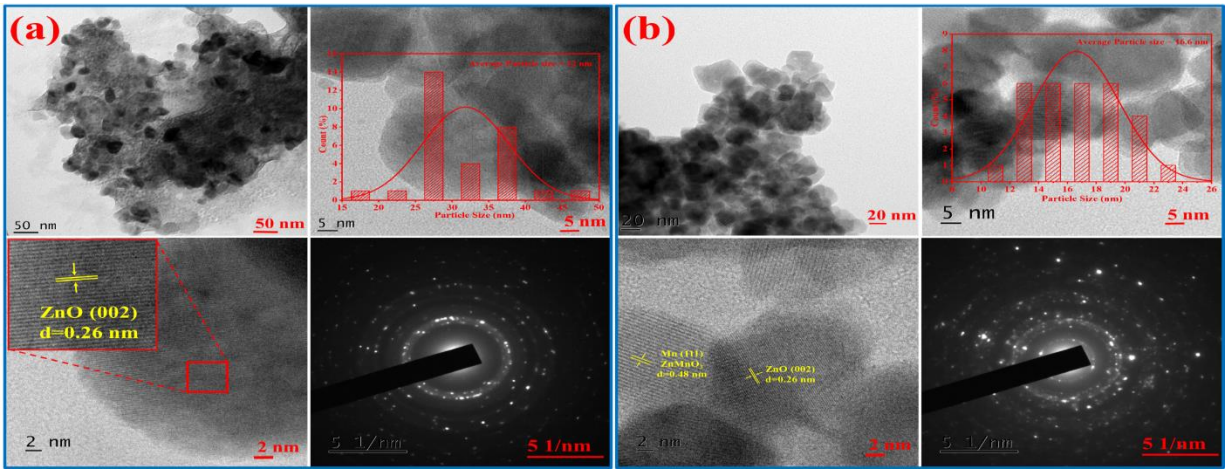

Figure 4. HRTEM-SAED images of (a) pure ZnO and (b) Mn5%-ZnO.

The fig. 4b reveals the size and sphere morphology of the Mn doped ZnO nanomaterials. The particle size of the Mn doped ZnO gets reduced while the inclusion of manganese ion with ZnO matrix. The fig. 4b evidenced that the particle size calculated from the histogram to be of 16.6 nm. The d-spacing for Mn5% doped ZnO nanospheres are calculated and there is two different lattice fringes in various directions were observed. The d-spacing for ZnO (002) plane is 0.26 nm and 0.48 nm for $ZnMnO_3$ (111) or $ZnMn_2O_4$ (101) which is in complimentary with the XRD results [25]. It indicates that the presence of Mn ions on the ZnO surface. The SAED pattern of Mn doped ZnO exhibits both concentrated ring and dot pattern reveals the highly crystalline behavior of the material. This enhanced crystalline nature of the materials is beneficial for photocatalytic applications [36].

Bandgap shift observation by UVDRS analysis.

The optical properties of Mn-doped ZnO microstructures were studied using UV-Vis diffuse reflectance spectroscopy (UV-DRS) in the 200–800 nm wavelength range. Both pure ZnO and Mn-ZnO samples showed good transparency in the visible spectrum (400–700 nm). Figures 5a and 5b display the UV-DRS absorbance spectra and Tauc plots for pure ZnO and Mn-ZnO with different doping concentrations (1%, 3%, and 5%) [37].

Journal of Chemical Health Risks

www.jchr.org

JCHR (2025) 15(1), 551-560 | ISSN:2251-6727

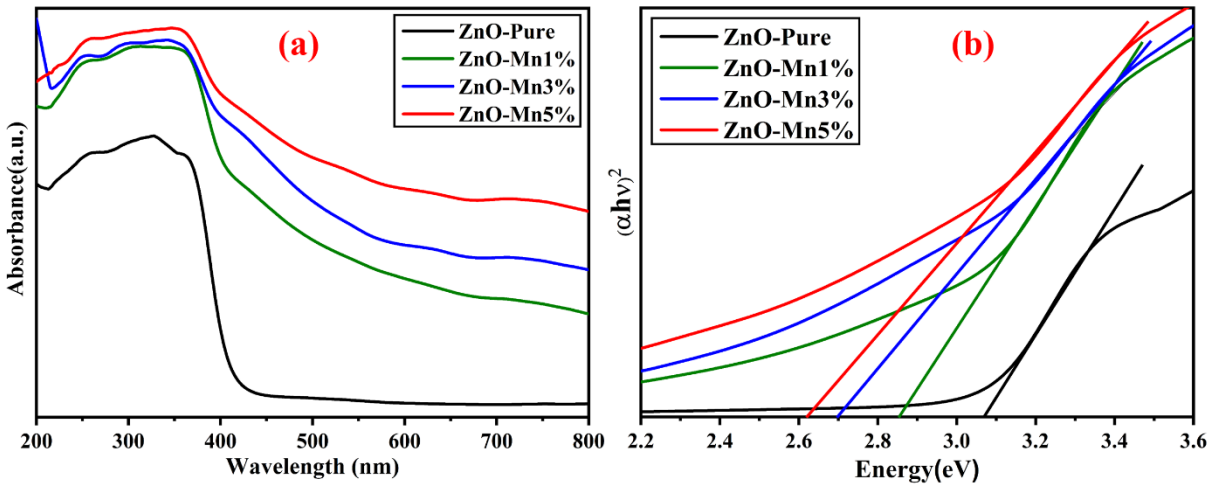

Figure 5. (a) UVDRS Absorbance plot, (b) Tauc plot of Pure and Mn doped ZnO (1, 3 and 5%).

The calculated bandgap values, determined from the Tauc plot, ranged from 3.07 eV to 2.62 eV slightly lower than the standard direct bandgap of 3.37 eV for bulk ZnO. Under UV exposure, defect states such as oxygen vacancies and interstitials can form or become activated in the band structure. These defects introduce intermediate energy levels within the bandgap, effectively lowering its energy. As a result, the material's absorption spectrum shifts toward longer wavelengths, causing a redshift. The bandgap values calculated using the Tauc plot are provided in Table. 1 [38].

BET Surface area analysis.

The BET analysis is widely used to evaluate the surface area and porosity of materials, which are critical for understanding their performance in photocatalysis. For Mn-doped ZnO (Mn5%-ZnO), the BET surface area analysis, along with N_2 adsorption-desorption isotherms, provides insights into its porous structure and active surface area. These properties directly influence the material efficiency in photocatalytic processes. The surface area and pore size were examined through BET N_2 sorption analysis at 77K and the results are depicted in fig. 6 and the values are given in table 1. Both the samples displayed type IV isotherms with H3 hysteresis loops, indicating the formation of parallel plate shaped pores during nitrogen adsorption and desorption, suggesting the presence pores in the synthesized materials [39].

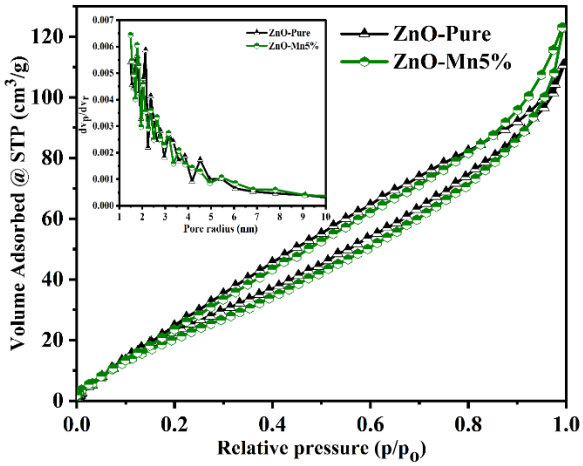

Figure 6. Surface area of Pure and Mn5% doped ZnO.

From the fig. 6 surface area of pure and Mn5% doped ZnO calculated to be 86 m^2/g and 90 m^2/g respectively. Using ethylene diamine the synthesis of pure and Mn doped samples were synthesized. In pure ZnO there is nucleation and agglomeration takes place in presence of structure directing amine and which results surface area of 86 m^2/g with 0.161 cm^3/g pore volume. When manganese included on ZnO surface there is a marginal increase in surface area 90 m^2/g and 0.185 cm^3/g pore volume is observed. This improved surface area and pore volume are responsible for active sites which facilitates enhanced photocatalytic activity in various applications like photocatalytic dye degradation and photocatalytic hydrogen production under visible light [40].

Journal of Chemical Health Risks

www.jchr.org

JCHR (2025) 15(1), 551-560 | ISSN:2251-6727

Photocatalytic Dye Degradation of Methylene Blue

The synthesized pure and Mn doped ZnO nanomaterials are potential photocatalysts for the degradation of MB dye. The photocatalytic activity of the pure and Mn5% doped ZnO are shown in fig. 7a and 7b respectively. From fig. 7c the degradation efficiency of both pure (87.2%) and Mn5%-ZnO (90.8%) are revealed.

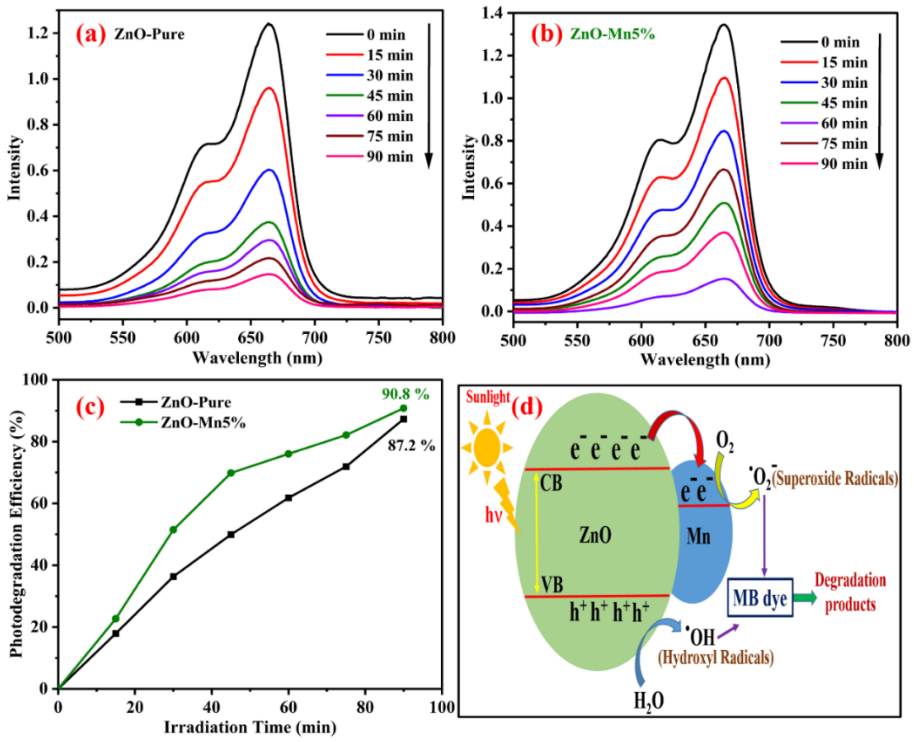

Figure 7. UV-Visible spectra of (a) Pure-ZnO, (b) Mn5%-ZnO, (c) Degradation efficiency and (d) Mechanism of methylene blue dye degradation.

Table. 1 Various parameters of the synthesized pure and Mn doped ZnO.

Sample	**Pure-ZnO**	**Mn5%-ZnO**
D from W-H plot (nm)	58	18
D from TEM (nm)	32	16.6
Bandgap (eV)	3.07	2.62
Surface area [S_{BET}] (m^2/g)	86	90
Pore radius (nm)	2.1	1.4
Pore volume (cm^3/g)	0.161	0.185
Degradation (%)	87.2	90.8

The schematic diagram of photocatalytic mechanism is represented in fig. 7d. In this, the fermi energy of Mn doped ZnO is lower than that pure ZnO material, causing electrons to move from ZnO to Mn [41]. Radical production is the primary mechanism behind the photodegradation of MB dye using pure and Mn doped ZnO photocatalyst. The highly reactive radicals generated in the solution attack the dye molecules, resulting in less toxic by products such as water and carbon dioxide. The enhanced adsorption of reactants and light absorption leads to the efficient generation of ROS like hydroxyl radicals (•OH) and superoxide anions (O_2^{-}•), which are responsible for degrading organic pollutants [42].

CONCLUSIONS

The structure directing amine mediated synthesis of Mn doped ZnO nanospheres by hydrothermal method was investigated. From the XRD analysis the phase purity and hexagonal wurtzite structure of the synthesized samples were confirmed and matched with JCPDS file.

Journal of Chemical Health Risks

www.jchr.org

JCHR (2025) 15(1), 551-560 | ISSN:2251-6727

The crystallite size calculated by W-H plot method and it is reduced from 58 nm to 18 nm when Mn doped with ZnO There are some secondary XRD peaks also detected when Mn introduced on ZnO surface which indicates the presence of Mn ions on the ZnO surface. From the FTIR analysis ZnO vibration and Mn-O peaks are witnessed. The UVDRS investigation reveals the bandgap of pure is around 3.07 eV and for Mn doped ZnO is 2.62 eV. This bandgap engineering through metal doping will enhance the visible light activity of the material. Nanospheres developed as microrod morphology of the pure and Mn doped samples were examined by HRSEM analysis and the elemental composition of the Zn, O and Mn were analyzed. HRTEM analysis confirms the nanosphere morphology and the particle size distribution histogram reveals size of pure ZnO is to be 32 nm and 16.6 nm for Mn5% doped ZnO. From the BET analysis the increased surface area and pore volume of the synthesized Mn doped ZnO is about 90 m^2/g. This increased surface area will beneficial for enhanced light harvesting ability and it will create more active sites for photocatalytic applications. The photocatalytic dye degradation of methylene blue dye analyzed by UV visible studies which reveals 90.8% of photocatalytic degradation efficiency of methylene blue dye under visible light condition this feature will protect the environment.

ACKNOWLEDGMENTS

Author K. Sasikumar acknowledges Sacred Heart College (Autonomous), Tirupattur for XRD and FTIR Instrument facilities.

ASSOCIATED CONTENT

Notes

The authors declare no known competing interest.

REFERENCES

1. Dong, S.; Feng, J.; Fan, M.; Pi, Y.; Hu, L.; Han, X.; Liu, M.; Sun, J.; Sun, J., Recent developments in heterogeneous photocatalytic water treatment using visible light-responsive photocatalysts: a review. *RSC Advances* **2015,** *5* (19), 14610-14630.
2. Kumar, S. G.; Rao, K. S. R. K., Zinc oxide based photocatalysis: tailoring surface-bulk structure and related interfacial charge carrier dynamics for better environmental applications. *RSC Advances* **2015,** *5* (5), 3306-3351.
3. Shaham Waldmann, N.; Paz, Y., Photocatalytic Reduction of Cr (VI) by Titanium Dioxide Coupled to Functionalized CNTs: An Example of Counterproductive Charge Separation. *The Journal of Physical Chemistry C* **2010,** *114* (44), 18946-18952.
4. Hariharan, C., Photocatalytic degradation of organic contaminants in water by ZnO nanoparticles: Revisited. *Applied Catalysis A: General* **2006,** *304*, 55-61.
5. Tian, C.; Zhang, Q.; Wu, A.; Jiang, M.; Liang, Z.; Jiang, B.; Fu, H., Cost-effective large-scale synthesis of ZnO photocatalyst with excellent performance for dye photodegradation. *Chemical Communications* **2012,** *48* (23), 2858-2860.
6. Achouri, F.; Corbel, S.; Aboulaich, A.; Balan, L.; Ghrabi, A.; Ben Said, M.; Schneider, R., Aqueous synthesis and enhanced photocatalytic activity of ZnO/Fe_2O_3 heterostructures. *Journal of Physics and Chemistry of Solids* **2014,** *75* (10), 1081-1087.
7. Moussa, H.; Girot, E.; Mozet, K.; Alem, H.; Medjahdi, G.; Schneider, R., ZnO rods/reduced graphene oxide composites prepared via a solvothermal reaction for efficient sunlight-driven photocatalysis. *Applied Catalysis B: Environmental* **2016,** *185*, 11-21.
8. Jeena, V.; Robinson, R. S., Convenient photooxidation of alcohols using dye sensitised zinc oxide in combination with silver nitrate and TEMPO. *Chemical Communications* **2012,** *48* (2), 299-301.
9. Wang, F.; Liang, L.; Shi, L.; Liu, M.; Sun, J., CO_2-assisted synthesis of mesoporous carbon/C-doped ZnO composites for enhanced photocatalytic performance under visible light. *Dalton Transactions* **2014,** *43* (43), 16441-16449.
10. Anandan, S.; Miyauchi, M., Ce-doped ZnO (CexZn1−xO) becomes an efficient visible-light-sensitive photocatalyst by co-catalyst (Cu^{2+}) grafting. *Physical Chemistry Chemical Physics* **2011,** *13* (33), 14937-14945.
11. Ahmad, M.; Ahmed, E.; Zhang, Y.; Khalid, N. R.; Xu, J.; Ullah, M.; Hong, Z., Preparation

of highly efficient Al-doped ZnO photocatalyst by combustion synthesis. *Current Applied Physics* **2013,** *13* (4), 697-704.

12. Mohan, R.; Krishnamoorthy, K.; Kim, S.-J., Enhanced photocatalytic activity of Cu-doped ZnO nanorods. *Solid State Communications* **2012,** *152* (5), 375-380.
13. Bloh, J. Z.; Dillert, R.; Bahnemann, D. W., Transition metal-modified zinc oxides for UV and visible light photocatalysis. *Environmental Science and Pollution Research* **2012,** *19* (9), 3688-3695.
14. Erwin, S. C.; Zu, L.; Haftel, M. I.; Efros, A. L.; Kennedy, T. A.; Norris, D. J., Doping semiconductor nanocrystals. *Nature* **2005,** *436* (7047), 91-94.
15. Kuriakose, S.; Satpati, B.; Mohapatra, S., Enhanced photocatalytic activity of Co doped ZnO nanodisks and nanorods prepared by a facile wet chemical method. *Physical Chemistry Chemical Physics* **2014,** *16* (25), 12741-12749.
16. Ullah, R.; Dutta, J., Photocatalytic degradation of organic dyes with manganese-doped ZnO nanoparticles. *Journal of Hazardous Materials* **2008,** *156* (1), 194-200.
17. Rekha, K.; Nirmala, M.; Nair, M. G.; Anukaliani, A., Structural, optical, photocatalytic and antibacterial activity of zinc oxide and manganese doped zinc oxide nanoparticles. *Physica B: Condensed Matter* **2010,** *405* (15), 3180-3185.
18. Mahmood, M. A.; Baruah, S.; Dutta, J., Enhanced visible light photocatalysis by manganese doping or rapid crystallization with ZnO nanoparticles. *Materials Chemistry and Physics* **2011,** *130* (1), 531-535.
19. Zhang, D., Structural, optical, electrical, and photocatalytic properties of manganese doped zinc oxide nanocrystals. *Russian Journal of Physical Chemistry A* **2012,** *86* (1), 93-99.
20. Yang, Y.; Li, Y.; Zhu, L.; He, H.; Hu, L.; Huang, J.; Hu, F.; He, B.; Ye, Z., Shape control of colloidal Mn doped ZnO nanocrystals and their visible light photocatalytic properties. *Nanoscale* **2013,** *5* (21), 10461-10471.
21. Saleh, R.; Djaja, N. F., Transition-metal-doped ZnO nanoparticles: Synthesis, characterization and photocatalytic activity under UV light. *Spectrochimica Acta Part A: Molecular and Biomolecular Spectroscopy* **2014,** *130*, 581-590.
22. Umar, K.; Aris, A.; Parveen, T.; Jaafar, J.; Abdul Majid, Z.; Vijaya Bhaskar Reddy, A.; Talib, J., Synthesis, characterization of Mo and Mn doped ZnO and their photocatalytic activity for the decolorization of two different chromophoric dyes. *Applied Catalysis A: General* **2015,** *505*, 507-514.
23. Mohamed, A.; El-Sayed, R.; Osman, T. A.; Toprak, M. S.; Muhammed, M.; Uheida, A., Composite nanofibers for highly efficient photocatalytic degradation of organic dyes from contaminated water. *Environmental Research* **2016,** *145*, 18-25.
24. Biswas, B. D.; Purkayastha, M. D.; Tiwari, E.; Denrah, S.; Sarkar, M.; Darbha, G. K.; Majumder, T. P., Study of the photocatalytic activity of Mn-doped ZnO nanocomposites depending on their morphology and structure with the variation of manganese concentration. *Surfaces and Interfaces* **2021,** *23*, 100902.
25. Sambandam, B.; Michael, R. J. V.; Manoharan, P. T., Oxygen vacancies and intense luminescence in manganese loaded Zno microflowers for visible light water splitting. *Nanoscale* **2015,** *7* (33), 13935-13942.
26. Li, X.; Zhu, X.; Jin, K.; yang, D., Study on structural and optical properties of Mn-doped ZnO thin films by sol-gel method. *Optical Materials* **2020,** *100*, 109657.
27. Vijayaprasath, G.; Murugan, R.; Asaithambi, S.; Sakthivel, P.; Mahalingam, T.; Hayakawa, Y.; Ravi, G., Structural and magnetic behavior of Ni/Mn co-doped ZnO nanoparticles prepared by co-precipitation method. *Ceramics International* **2016,** *42* (2, Part A), 2836-2845.
28. Achouri, F.; Corbel, S.; Balan, L.; Mozet, K.; Girot, E.; Medjahdi, G.; Said, M. B.; Ghrabi, A.; Schneider, R., Porous Mn-doped ZnO nanoparticles for enhanced solar and visible light photocatalysis. *Materials & Design* **2016,** *101*, 309-316.
29. Lafta, A.; Alsultani, A.; Saleh Farhood, A., Modification of the Photocatalytic Activity of Zinc Oxide by Doping Silver. *International*

Journal of Chemical Health Risks

www.jchr.org

JCHR (2025) 15(1), 551-560 | ISSN:2251-6727

Journal of Science and Research (IJSR) **2014,** *3*, 2133-2138.

30. Alshamsi, H.; Hussein, B., Hydrothermal Preparation of Silver Doping Zinc Oxide Nanoparticles: Studys, Characterization and Photocatalytic Activity. *Oriental Journal of Chemistry* **2018,** *34*.
31. Gu, P.; Zhu, X.; Yang, D., Structural, optical and photoelectric properties of Mn-doped ZnO films used for ultraviolet detectors. *RSC Advances* **2019,** *9* (14), 8039-8047.
32. Ghica, D.; Vlaicu, I. D.; Stefan, M.; Nistor, L. C.; Nistor, S. V., On the agent role of Mn^{2+} in redirecting the synthesis of $Zn(OH)^2$ towards nano-ZnO with variable morphology. *RSC Advances* **2016,** *6* (108), 106732-106741.
33. Putri, N. A.; Fauzia, V.; Iwan, S.; Roza, L.; Umar, A. A.; Budi, S., Mn-doping-induced photocatalytic activity enhancement of ZnO nanorods prepared on glass substrates. *Applied Surface Science* **2018,** *439*, 285-297.
34. Ayu, D. G.; Gea, S.; Andriayani; Telaumbanua, D. J.; Piliang, A. F. R.; Harahap, M.; Yen, Z.; Goei, R.; Tok, A. I. Y., Photocatalytic Degradation of Methylene Blue Using N-Doped ZnO/Carbon Dot (N-ZnO/CD) Nanocomposites Derived from Organic Soybean. *ACS Omega* **2023,** *8* (17), 14965-14984.
35. Truong, T. K.; Van Doan, T.; Tran, H. H.; Van Le, H.; Lam, V. Q.; Tran, H. N.; Cao, T. M.; Van Pham, V., Effect of Cr Doping on Visible-Light-Driven Photocatalytic Activity of ZnO Nanoparticles. *Journal of Electronic Materials* **2019,** *48* (11), 7378-7388.
36. Al-Mamun, M. R.; Iqbal Rokon, M. Z.; Rahim, M. A.; Hossain, M. I.; Islam, M. S.; Ali, M. R.; Bacchu, M. S.; Waizumi, H.; Komeda, T.; Hossain Khan, M. Z., Enhanced photocatalytic activity of Cu and Ni-doped ZnO nanostructures: A comparative study of methyl orange dye degradation in aqueous solution. *Heliyon* **2023,** *9* (6), e16506.
37. Sivaranjani, K.; Sivakumar, S.; Dharmaraja, J., Enhancement Photocatalytic Activity of Mn Doped Cds/Zno Nanocomposites for the Degradation of Methylene Blue Under Solar Light Irradiation. *Advances in Materials Science* **2022,** *22* (2), 28-48.
38. Shao, D.; Sun, H.; Gao, J.; Xin, G.; Anthony Aguilar, M.; Yao, T.; Koratkar, N.; Lian, J.; Sawyer, S., Flexible, thorn-like ZnO-multiwalled carbon nanotube hybrid paper for efficient ultraviolet sensing and photocatalyst applications. *Nanoscale* **2014,** *6* (22), 13630-13636.
39. Li, W.; Wang, G.; Chen, C.; Liao, J.; Li, Z., Enhanced Visible Light Photocatalytic Activity of ZnO Nanowires Doped with Mn^{2+} and Co^{2+} Ions. *Nanomaterials* **2017,** *7* (1), 20.
40. Ahmad, M.; Ahmed, E.; Ahmed, W.; Elhissi, A.; Hong, Z. L.; Khalid, N. R., Enhancing visible light responsive photocatalytic activity by decorating Mn-doped ZnO nanoparticles on graphene. *Ceramics International* **2014,** *40* (7, Part A), 10085-10097.
41. Amrute, V.; Monika; Supin, K. K.; Vasundhara, M.; Chanda, A., Observation of excellent photocatalytic and antibacterial activity of Ag doped ZnO nanoparticles. *RSC Advances* **2024,** *14* (45), 32786-32801.
42. A, D.; Yadav, R.; C, S. P., An Eco-approach synthesis of undoped and Mn doped ZnO nano-photocatalyst for prompt decoloration of methylene blue dye. *Materials Today: Proceedings* **2022,** *48*, 494-501.